Structural deterioration of well-faceted MOFs upon H_2S exposure and its effect in the adsorption performance

Snezana Reljic,[a] Anna Broto-Ribas,[b] Carlos Cuadrado-Collados,[a] Erika O. Jardim,[a] Daniel Maspoch,[b,c] Inhar Imaz,[b] and Joaquin Silvestre-Albero*[a]

[a] S. Reljic, C. Cuadrado-Collados, Dr. E.O. Jardim, Prof. J. Silvestre-Albero
Laboratorio de Materiales Avanzados, Departamento de Química Inorgánica-IUMA
Universidad de Alicante
Ctra. San Vicente-Alicante s/n, E-03690 San Vicente del Raspeig, Spain
E-mail: joaquin.silvestre@ua.es

[b] A. Broto-Ribas, Prof. D. Maspoch, Dr. I. Imaz
Catalan Institute of Nanoscience and Nanotechnology (ICN2), CSIC and Barcelona Institute of Science and Technology,
Campus UAB, Bellaterra 08193, Barcelona, Spain

[c] Prof. D. Maspoch
ICREA
Pg. Lluís Companys 23, 08010 Barcelona, Spain

Supporting information for this article is given via a link at the end of the document.

Abstract: The structural deterioration of archetypical, well-faceted metal organic frameworks (MOFs) has been evaluated upon exposure to an acidic environment (H_2S). Experimental results show that the structural damage highly depends on the nature of the hybrid network (e.g., softness of the metal ions, hydrophilic properties, among others) and the crystallographic orientation of the exposed facets. Microscopy images show that HKUST-1 with well-defined octahedral (111) facets is completely deteriorated, ZIF-8 with preferentially exposed (110) facets exhibits a large external deterioration with the development of holes or cavities in the mesoporous range, whereas UiO-66-NH_2 with (111) exposed facets, and PCN-250 with (100) facets does not reflect any sign of surface damage. Despite the selectivity in the external deterioration, X-ray diffraction and gas adsorption measurements confirm that indeed all MOFs suffer an important internal deterioration, these effects being more severe for MOFs based on softer cations (e.g., Cu-based HKUST-1 and Fe-based PCN-250). These structural changes have inevitable important effects in the final adsorption performance for CO_2 and CH_4 at low and high pressures.

Introduction

The design of nanoporous materials able to store a large quantity of CH_4 and CO_2 at high pressure is one of the main challenges nowadays in materials science due to the necessity to combine: i) a widely developed porous structure; ii) a proper pore architecture (pore size and shape), able to promote a dense packing density of the adsorbed phase; iii) a large framework density, to achieve an optimum adsorption capacity in the minimum volume (v/v); and iv) a proper structural stability and cyclability. Previous studies described in the literature show that activated carbon materials and metal-organic frameworks (MOFs) are currently the most promising candidates for CH_4 and CO_2 storage due to the possibility to tune their porous network to achieve a proper adsorption performance.[1-10] In the specific case of CH_4, high-pressure adsorption measurements have shown that properly designed high-surface area carbon materials can reach the actual DoE target (i.e., 263 v/v) at 10 MPa and 25ºC.[11] These carbon materials also possess a proper performance for CO_2 capture at 5.0 MPa with an adsorption capacity above 2065 mg/g at 25ºC.[12] Despite these excellent values, the main drawback when working with activated carbon materials is the difficulty to tune a specific pore size and shape to achieve an optimum adsorption performance. Higher adsorption values have been described in the literature for MOFs due to the presence of a regular, well-defined porous network. Pen *et al.* reported a storage capacity for methane as high as 230 v/v at 3.5 MPa and 270 v/v at 6.5 MPa for HKUST-1.[4] Unfortunately, this excellent performance could not be preserved after a conforming step due to the mechanical collapse of the internal porous structure. More recently, Tian *et al.* reported the successful development of HKUST-1 monoliths with a storage capacity as large as 259 v/v at 6.5 MPa, avoiding the aforementioned limitations related with densification and shaping.[13] A similar approach was applied by Connolly *et al.* to grow UiO-66 monoliths with an exceptional performance for CH_4, up to 211 v/v at 6.5 MPa, and for CO_2 adsorption, up to 284 v/v at 4.0 MPa.[14]

Despite these excellent numbers, preferentially when using MOFs, one has to be aware that these experiments are always performed using high-purity gases. However, real industrial streams contain other gases that are able, not only to compete for the active sites, but also to deteriorate the quality of the porous network after use. For instance, this is the case of acidic molecules such as H_2S. H_2S is traditionally present in natural gas streams, in which, although methane is the main component, there is usually a H_2S content of <1.0 % vol. H_2S is also present in flue gas streams (in addition to CO_2, coal fired flue gas contains around 100 ppm H_2S) and in biogas (in addition to CH_4 and CO_2, biogas contains <3% of H_2S).

To date, some previous studies have already shown that exposure of MOFs to acidic gases can give rise to important structural changes.[15,16] Interestingly, the activation energy associated with these gas-framework interactions, and the associated side-effects, highly depends on the crystallographic

orientation. For instance, Pang *et al.* demonstrated that the (110) facets of ZIF-8 crystals are more reactive than the (100) facets under humid SO_2.[15] Furthermore, while this structural damaged was mainly restricted to the external surface of ZIF-8 crystals, the bulk of these crystals remained mainly unchanged. Remarkably, Dutta *et al.* reported that the bulk properties of ZIF-8 were preserved after exposing it to H_2S, showing similar intraparticle diffusivities before and after acid treatment.[16] Anisotropic acid etching of MOFs using HCl has also been used in the literature to obtain unprecedented morphologies due to the different reactivity among crystallographic directions.[17] These preliminary studies clearly anticipate that the composition of the effluent gas and, more specifically, the presence of acidic contaminants can have a crucial role in the performance and lifetime of MOFs. However, the effect that exposure to these acidic gases could have in the subsequent adsorption performance for the main constituents of the industrial effluents containing H_2S, i.e. CH_4 and CO_2, have been scarcely evaluated in the literature.

Based on these premises, the main goal of this study is to evaluate the structural deterioration of four archetypical, well-faceted MOFs (ZIF-8, UiO-66-NH_2, PCN-250 and HKUST-1) upon H_2S exposure under industrially relevant experimental conditions, and the subsequent evaluation of their adsorption performance for two relevant industrial/technological processes: CO_2 capture and CH_4 storage at high pressures. At this point it is important to highlight that, although some of them are not the best performing MOFs for this specific application, they constitute representative examples of the four main families of metallic nodes in MOFs (Zn-, Fe-, Zr- and Cu-based materials). In addition, they can be prepared with a high crystallographic quality and with well-defined facets, thus allowing a better understanding of external and internal deterioration effects.

Results and Discussion

External deterioration upon H_2S exposure.

One of the main characteristics of the four MOFs selected is the possibility to synthesize them in well-defined shapes with preferential orientation of specific crystallographic facets. This approach is of paramount importance to identify the selective attack of the acidic moieties to specific crystallographic domains. Figure 1 and 2 show FE-SEM images of the four MOFs before and after their exposure to H_2S for 10 h at 75ºC (in the case of HKUST-1 exposure was limited to 25ºC for 3h because these conditions were sufficient to cause a severe structural deterioration). As shown in Figure 1, the four as-synthesized MOFs possess different crystal sizes, shapes and morphologies. ZIF-8 is constituted by ~ 0.5 μm in-size rhombic dodecahedral particles exposing twelve (100) facets.[17] UiO-66-NH_2 exhibits uniform octahedral crystals with eight exposed (111) surfaces and an average crystal size of ~ 0.6 μm. PCN-250 is made of cubic crystals exposing six (100) facets with an average crystal size of ~ 1 μm. Although PCN-250 crystals are also quite uniform, smaller nanocrystals could be found attached to the main crystal units. Finally, HKUST-1 exhibits well-defined octahedral crystals with (111) exposed facets and an average crystal size of ~ 15 μm.

After exposure to H_2S, the situation differed depending on the MOF evaluated. Thus, while UiO-66-NH_2 and PCN-250 did not reflect external structural damages after H_2S exposure at 75ºC for 10 h, ZIF-8 started showing the formation of holes at the boundaries between (110) facets even after 3 h at 75ºC (Figure 2a). Notably, a further treatment of ZIF-8 crystals with H_2S for 10 h gave rise to more severe changes on the external surface of the (110) facets, with the creation of meso and macrocavities (Figure 2b). The limiting case is HKUST-1. For this specific sample, even 3h at 25ºC are sufficient to produce a drastic deterioration in the morphology of the crystals, with a complete destruction of the well-defined facets (Figure 2e).

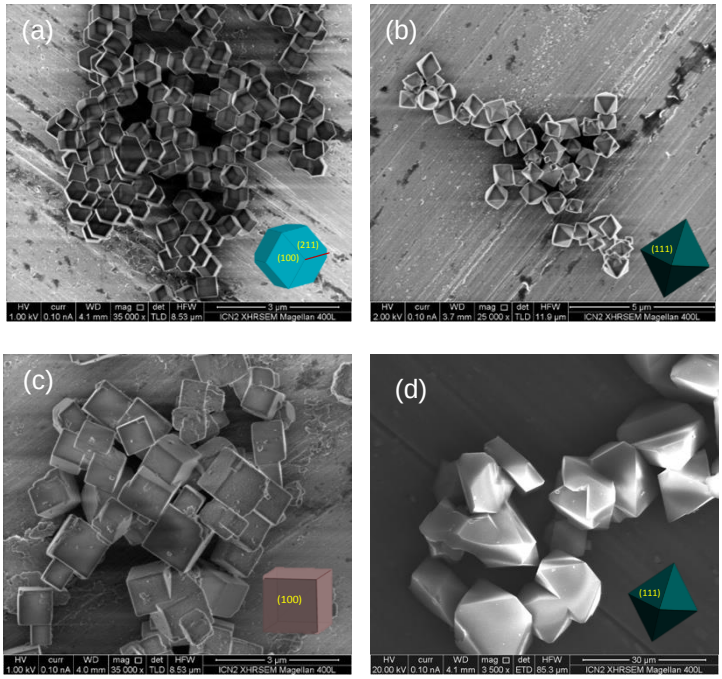

Figure 1. Representative FE-SEM images of as-synthesized (a) ZIF-8, (b) UiO-66-NH_2, (c) PCN-250 and (d) HKUST-1.

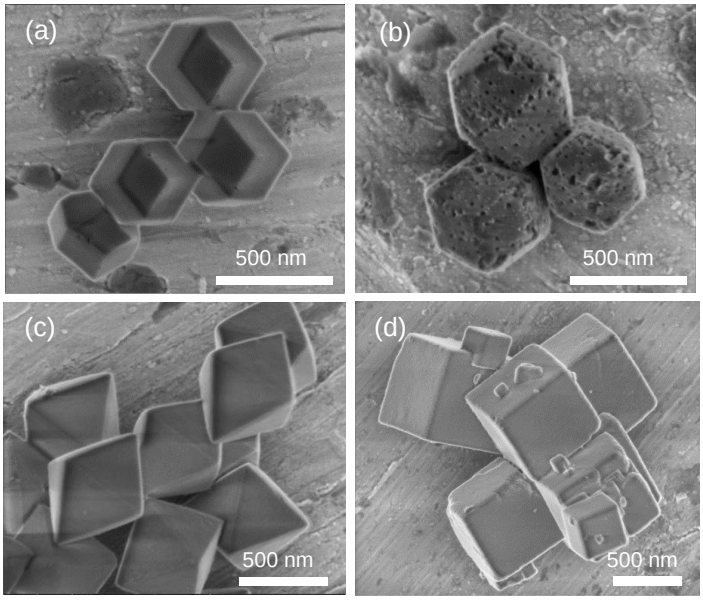

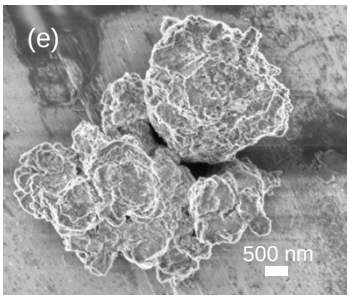

Figure 2. Representative FE-SEM images of (a,b) ZIF-8, (c) UiO-66-NH_2, (d) PCN-250 and (e) HKUST-1 after exposure to H_2S at 75ºC for 10 h. Note that image (a) was taken after a H_2S exposure at 75ºC for 3 h and (e) was taken after a H_2S exposure at 25ºC for 3h.

These results clearly show that the external deterioration of MOF crystals upon exposure to an acidic media depends, not only on the crystallographic orientation, but also on the nature of the MOF. While UiO-66-NH_2 and PCN-250 with exposed (111) and (100) facets, respectively, are highly resistant and does not experience visual damage, the (110) facets exposed in ZIF-8 are more prone to suffer severe damage with the development of highly extended nanometer size holes and cavities. This external deterioration of ZIF-8 crystals is in close agreement with recent results from Dutta *et al.*[16] In the case of HKUST-1, despite sharing a similar crystal morphology to UiO-66-NH_2, with eight well-defined (111) facets, FE-SEM results clearly anticipate a drastic deterioration of the crystal network even after exposure to H_2S at 25ºC for 3h. This observation anticipates the crucial role of the MOF nature, and more specifically, of the metallic nodes defining the extend of the structural deterioration in an acidic environment.

X-ray powder diffraction (XRPD) study of the internal deterioration.

One of the main questions when MOF crystals are exposed to acidic gases is the preservation of their quality after the different treatments. As abovementioned, FE-SEM characterization suggested the preservation of the crystal quality for both UiO-66-NH_2 and PCN-250, at least from a surface perspective. However, MOF crystals can also suffer internal deterioration, which detection requires the use of bulk techniques. To start evaluating the internal deterioration of our selected MOFs, we performed XRPD measurement before and after exposure of the four MOFs to an H_2S flow at different times (3 and 10 h) and temperatures (25 and 75ºC) (except for HKUST-1). As it can be appreciated in Figure 3, the patterns of the as-synthesized samples perfectly fit with the simulated patterns, thus confirming their purity. In the case of ZIF-8, H_2S exposure did not produce important changes in the XRPD pattern, except a broadening of the main diffraction peaks and a slight shift to higher angles. The internal deterioration *via* amorphization of the framework was more evident in UiO-66-NH_2, mainly at 75ºC, at which a significant decrease of intensity and a shift of the main XRPD peaks were observed. A similar amorphization was also found for PCN-250 upon H_2S exposure, mainly at 75ºC. In this latter case, a more pronounced shift and a decrease of the intensity of the XRPD peaks were clearly seen. Last but not least, XRPD analysis of HKUST-1 clearly anticipate that exposure to H_2S for 3h at 25ºC are sufficient to completely deteriorate the quality of the crystals, with a complete wash-out of the main XRPD contributions. Based on these observations, HKUST-1 exposure to H_2S was not tested for higher temperatures and/or longer times.

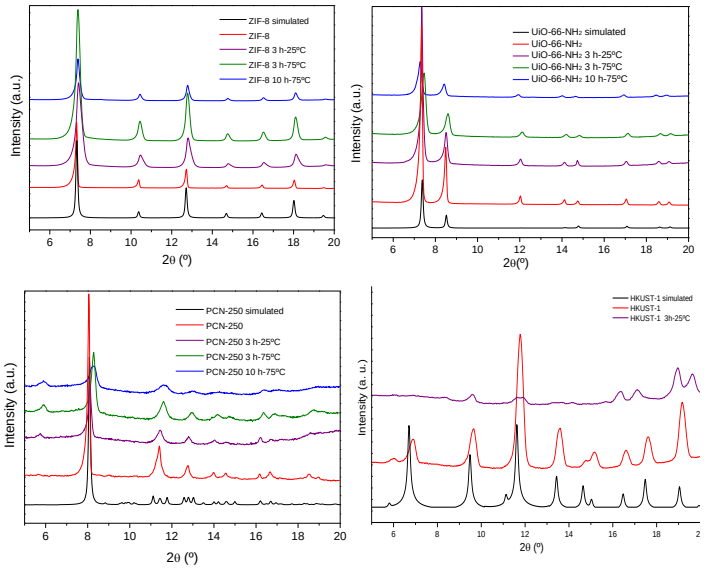

Figure 3. XRPD patterns for ZIF-8, UiO-66-NH_2, PCN-250 and HKUST-1 before and after exposure to H_2S.

It is important to highlight here that, contrariwise to the FE-SEM analysis described above, XRPD anticipates that the framework damage is more evident for UiO-66-NH_2 and PCN-250 than for ZIF-8. Thus, both techniques are complementary but necessary to evaluate the internal and external deterioration of MOFs upon H_2S exposure. They showed that the acid treatment clearly affects the external surface of ZIF-8 crystals but not their inner core. However, for UiO-66-NH_2 and PCN-250, while there is no evidence of external deterioration upon H_2S exposure, XRPD anticipates a certain degree of internal deterioration, which is more pronounced for PCN-250.

Textural characteristics before and after H_2S exposure.

A very important aspect when a porous material is exposed to acid gases is to ascertain its textural deterioration, i.e. the selective destruction of pores or cavities and/or the creation of new pores. These details can provide further insight about the reaction mechanism with the exposed gases. One of the main techniques for the characterization of the porous structure in nanoporous solids is gas adsorption at cryogenic temperatures. Among the different probe molecules available, N_2 adsorption at -196ºC is the most widely applied to evaluate both micro- and mesoporosity.[18] Figure 4 shows the N_2 adsorption isotherms for the four MOFs before and after exposure to H_2S under different experimental conditions. Note that, for ZIF-8, the isotherm was plotted in logarithmic scale for a more careful evaluation of the characteristic gate-opening effect taken place at mid-relative pressures.[19,20]

From these measurements, we found that the structural damage after exposure to H_2S highly depends on the nature of the MOF

material and the presence of functionalities in the organic linker. For ZIF-8, N_2 adsorption data revealed a progressive deterioration in the textural parameters (see Table S1 for further details), mainly due to the degradation of the microporous network. The pore size distribution (Figure S1) confirm the degradation of the microporous network and the development of new pores around 1.8-2 nm. Furthermore, the apparent surface area decreased up to 16% after a H_2S treatment at 75ºC for 10 h, from an initial value of 1860 m^2/g down to a value of 1560 m^2/g. A closer look to the N_2 isotherms (see inset) showed that the gate-opening behavior at p/p_0 ~ 0.01 does not change or shifts after the acid treatment, i.e., apparently the acid treatment produces an external deterioration of the crystal, without perturbation of the structural gate-opening phenomena.

Similarly, UiO-66-NH_2 suffered a progressive deterioration upon acid treatment; evidenced by the decrease of its apparent surface area from 1160 m^2/g (as-synthesized sample) to 1022 m^2/g after exposure to H_2S (75ºC, 10 h). A closer look to the textural values described in Table S2 showed that the deterioration affects preferentially to the microporous network, in close agreement with the N_2 isotherms. Interestingly, the structural deterioration after its exposure to H_2S (75ºC, 10 h) was the lowest among the evaluated MOFs (only 12%). This observation is in close agreement with the improved stability described by Mounfield *et al.* for NH_2-functionalized MIL-125 after exposure to humid SO_2.[21]

N_2 adsorption isotherms of PCN-250 after its exposure to H_2S showed an important deterioration of the framework with a significant shrinkage of the microporous network, and the associated development of mesocavities. Indeed, the apparent surface area decreased from 1300 m^2/g (as-synthesized MOF) down to 830 m^2/g upon the acid treatment for 10 h at 75ºC, i.e., a decrease of around 36%, much higher than that observed for ZIF-8 and UiO-66-NH_2. Furthermore, the mesopore volume scaled up to 0.14 cm^3/g. The development of mesopores with a wide pore size distribution (from 3.0 nm to 6.0 nm) can be more clearly appreciated in Figure S1.

Finally, when HKUST-1 was exposed to H_2S, 3h at 25ºC were sufficient to produce a complete collapse of the 3D network. As it can be observed in Figure 4 and Table S4, the nitrogen adsorption capacity decreases more than 95%, the BET surface area dropping from 1688 m^2/g in the original MOF down to 74 m^2/g in the treated sample.

In summary, the textural characterization of the four MOFs exposed to H_2S showed that all of them suffer somehow an important structural deterioration. These effects are more drastic for Cu(II)-based HKUST-1, followed by Fe(III)-based PCN-250, Zn(II)-based ZIF-8, and finally the more robust Zr(IV)-based UiO-66-NH_2. Although previous studies by Mounfield *et al.* demonstrated that amine functionalization can improve the structural stability of MIL-125 towards acidic gases,[21] our results suggest that the structural stability is also defined by the physicochemical properties of the MOF network. Our results suggest that the stability of the MOFs is largely defined by the acid-base interactions between the H_2S molecule and the MOF framework (HSAB concept), i.e., a soft base such as sulphur will have a higher affinity and will form stronger bonds with softer metal ions (transition metals with a high occupation of *d* orbitals). Based on these premises, sulphur should have higher affinity for softer cations (e.g., Cu(II), Zn(II) and Fe(III)) versus harder cations (e.g., Zr(IV)), thus explaining the observed stability trends. However, at this point we cannot exclude an additional contribution due to the hydrophilic character of the MOF, i.e., due to the presence of residual humidity in the material. Although Zn(II) is softer than Cu(II) and Fe(III), the hydrophobic character of ZIF-8 will prevent residual moisture to participate in the degradation mechanism, whereas this is not the case for PCN-250 and, even less, for the hydrophilic HKUST-1. Computational investigations by Pang et al. supported the reaction mechanism between the MOF framework and SO_2, and the promoting effect by water through the formation of H_2SO_3 species.[15] Similar experiment by Bhattacharyya et al. confirmed the larger structural deterioration in ZIF-8 under humid SO_2 conditions, compared to the same system in dry conditions.[22]

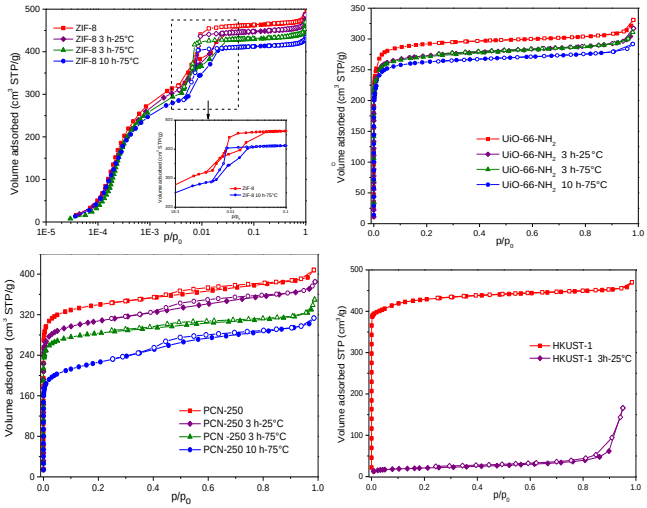

Figure 4. N_2 adsorption (full symbols)/desorption (empty symbols) isotherms for ZIF-8, UiO-66-NH_2, PCN-250 and HKUST-1 before and after exposure to H_2S.

X-ray photoelectron spectroscopy (XPS) analysis.

The chemical composition and environment of the four MOFs before and after the acidic treatment with H_2S were evaluated using X-ray photoelectron spectroscopy (XPS). XPS is a surface sensitive technique and consequently, it is suitable to evaluate the potential deterioration of the surface of the MOF crystals, since this is the most susceptible region upon H_2S exposure.

Table 1 reports the surface composition for ZIF-8, UiO-66-NH_2, PCN-250 and HKUST-1 before and after the thermal treatment at 75ºC for 10 h under H_2S flow conditions (in the case of HKUST-1 the data correspond to 25ºC for 3h). In the case of ZIF-8, the acid treatment gave rise to a decrease in the atomic % of carbon and nitrogen, whereas the oxygen content experienced a slight increase. These changes are clearly appreciated after normalization with the total amount of metal (M). Although these results could suggest that imidazole ligands are removed from the surface more efficiently than Zn(II) metallic nodes, in agreement with previous data reported in the literature, standard deviations are too large to provide a conclusive answer.[15] Compared to the literature, the increase in the amount of oxygen in our study was rather limited due to the dry nature of the H_2S stream used. The detailed spectra for the C 1s, N 1s, O 1s, S 2p and Zn 2p can be found in the Supporting Information (Figure S2-S5). These spectra confirmed the above described data and the presence of a significant amount of sulphur anchored to the ZIF-8 surface, with a peak centered at a

binding energy of ~ 162-163 eV (atomic % 0.7); very close to the binding energy of ZnS.[23] Exposure of ZIF-8 to H_2S also shifted the Zn $2p_{3/2}$ signal to higher binding energies (a shoulder appeared at ~ 1023.1 eV). This shift is most probably associated with Zn-S species. However, care must be taken in the interpretation of this data due to difficulty to differentiate the chemical state of Zn through the evaluation of the Zn $2p_{3/2}$ signal. Concerning UiO-66-NH_2, the XPS analysis showed that the surface of this material contains preferentially carbon and oxygen, with a small contribution of nitrogen (Figure S3 shows a detailed evaluation of these components). Upon H_2S exposure, the carbon and oxygen ratio (normalized to the amount of Zr) decreased, while the nitrogen ratio remains stable. These results support the hypothesis that the acid treatment promotes the deterioration of the ligand (maybe through acetate defects). Interestingly, the amount of sulphur retained by UiO-66-NH_2 after the acid treatment was negligible (atomic % = 0), thus confirming the weak affinity of sulphur for a hard metallic cation such as Zr.

Table 1. Chemical composition (carbon, oxygen, metal, nitrogen and sulphur content) of ZIF-8, UiO-66-NH_2,PCN-250 and HKUST-1 samples (atomic %) and atomic ratio, deduced from XPS analysis before and after their exposure to H_2S at 75ºC for 10 h (25ºC for 3h in the case of HKUST-1).

Sample		C (%)	O (%)	M[a] (%)	N (%)	S (%)	C/M	N/M	O/M
ZIF-8	Before	75.6 ±1.2	5.1 ±0.7	4.2 ±1.2	15.1 ±3.7	0 ±0.0	18.1	3.6	1.2
	After	72.4 ±1.0	7.4 ±0.5	4.8 ±0.5	14.6 ±1.0	0.7 ±0.1	14.9	3.0	1.5
UiO-66-NH_2	Before	73.4 ±0.4	20.7 ±0.0	3.4 ±0.1	2.5 ±0.3	0 ±0.0	21.8	0.74	6.2
	After	67.9 ±3.9	24.3 ±2.4	4.5 ±1.1	3.1 ±0.6	0.2 ±0.1	14.9	0.70	5.3
PCN-250	Before	72.3 ±3.4	22.5 ±2.6	1.7 ±0.6	3.0 ±0.1	0 ±0	42.5	1.8	13.2
	After	74.0 ±4.5	20.5 ±4.1	2.0 ±0.2	2.5 ±1.1	0.9 ±0.3	37.0	1.2	10.2
HKUST-1	Before	65.0 ±0.1	27.8 ±0.7	6.4 ±0.5	0.45 ±0.1	0 ±0.0	10.1	0.07	4.3
	After	53.5 ±2.7	36.3 ±2.1	6.5 ±0.8	0.36 ±0.1	3.2 ±0.1	8.3	0.06	5.6

[a] M corresponds to the different metals in the MOFs, i.e. Zn for ZIF-8, Zr for UiO-66-NH_2, Fe for PCN-250 and Cu for HKUST-1.

PCN-250 also contains a significant amount of carbon, oxygen and nitrogen. However, the acid treatment significantly decreased the amount of these three components referred to Fe, as shown in Table 1. The evaluation of the Fe 2p signal in the as-synthesized PCN-250 showed a broad band centered at 711.7 eV (Figure S4), which was attributed to Fe(III). After exposure to H_2S, the main contribution developed a shoulder at lower binding energies (*ca*. 709.7 eV), due to the development of Fe-S species.[24,25] The retention of sulphur in the MOF network was clearly appreciated in the S $2p^3$ region with a significant contribution at 164 eV (0.9 at.%), attributed to the formation of Fe-based thiol (-SH) or disulfide (S^{2-}) species.

Finally, HKUST-1 exhibits a significant content of carbon and oxygen in the as-prepared sample, whereas nitrogen content is negligible. However, upon H_2S exposure the chemical analysis shows a significant decrease in the amount of carbon and a large increase in the oxygen content, most probably associated with the formation of -OH surface species promoted by moisture. As expected, the amount of sulphur incorporated in HKUST-1 is the highest among of samples evaluated (up to 3.2 wt.%), in close agreement with the softer character of the Cu metallic nodes.

High-pressure CO_2 adsorption isotherms.

One of the open questions at this point is how these structural changes produced by an acidic environment can alter the adsorption performance of these MOFs for two industrially relevant gases, i.e. CH_4 and CO_2. Previous studies described in the literature using carbide-derived carbons (TiC-CDC) have anticipated that CO_2 adsorption at atmospheric pressure (0.1 MPa) requires the presence of pores around 0.8 nm in size; i.e., angstrom-size pores allow an optimum packing density under these experimental conditions.[26] However, larger pores (around 2.0-3.0 nm) govern the adsorption performance for high-pressure applications.[27] Based on these premises, although deterioration of the microporous structure in MOFs must be *a priori* detrimental for the adsorption of CO_2 at atmospheric pressure, the potential development of mesopores, through the destruction of micropores, can be useful to promote the adsorption at high pressures.

Figure 5 shows the CO_2 excess adsorption isotherms at 25ºC and up to 4.0 MPa for the four MOFs before and after exposure to an acidic environment. As it can be appreciated, the as-synthesized MOFs exhibit a type I isotherm with a large adsorption capacity at low pressures due to the presence of microporosity and a certain increased capacity above 3.0 MPa; most probably due to the presence of mesocavities in the interparticle space. The total adsorption capacity for CO_2 at 4.0 MPa is 435 mg/g for ZIF-8, 505 mg/g for UiO-66-NH_2, 635 mg/g for PCN-250 and 700 mg/g for HKUST-1. These values are in the same range observed for carbon materials exhibiting exclusively micropores,[27] and much lower than those reported for high-surface area carbon materials and exceptional MOFs (values larger than 1200 mg/g have been reported for samples like carbon VR-5, MOF-177, and MOF-200, at 4.0 MPa).[12,28,29]

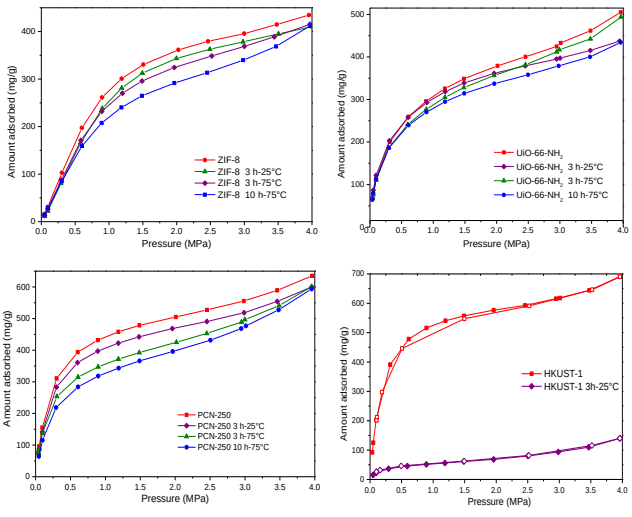

Figure 5. High-pressure CO_2 adsorption isotherms (mg/g) at 25ºC for ZIF-8, UiO-66-NH_2, PCN-250 and HKUST-1 evaluated before and after exposure to H_2S.

After exposure to an acidic environment, the four MOFs exhibited a market decrease in the amount adsorbed, preferentially at pressure below 2.0 MPa, due to the deterioration of the inner microporous network. This reduction was significant for ZIF-8 and PCN-250, with a decrease in the amount adsorbed at 2.0 MPa of around 20% for the sample exposed at 75ºC for 10 h (see Tables S5-S8). In these two MOFs, however, the decrease in the adsorption capacity upon H_2S exposure was less significant at 4.0 MPa; this value being around 5-6 % compared to the un-treated ZIF-8 and PCN-250. In the case of UiO-66-NH_2, the decrease in the amount of CO_2 adsorbed was larger at higher pressures, whereas at 2.0 MPa, the effect is rather limited. This observation reflects the lower deterioration of the microporous structure in UiO-66-NH_2, in close agreement with the N_2 adsorption data described above. On the contrary, the development of mesocavities or holes in ZIF-8 and PCN-250 upon deterioration explains the additional increase in the amount of CO_2 adsorbed above 3.0 MPa. HKUST-1 constitutes an exception to the observed behavior. In this sample, after H_2S exposure, a drastic decrease in the amount of CO_2 adsorbed can be appreciated over the whole pressure range evaluated (at 4.0 MPa CO_2 uptake does not reach 150 mg/g).

High-pressure CH_4 adsorption isotherms.

Another important adsorption process susceptible of acid contamination is CH_4 storage, either from natural gas or biogas. Although the amount of H_2S in these streams can be reduced to ppm levels using a proper guard bed, the presence of traces of H_2S or any other acid molecule can have a tremendous impact in the adsorption performance of the porous material after several cycles. To this end, excess methane adsorption capacity was also evaluated for the four MOFs at 25ºC and up to 4.0 MPa. Under these experimental conditions and contrary to CO_2, only micropores must be susceptible to participate in the adsorption process. This assumption is based on the large difference in the critical temperature between the two probe molecules: CO_2 (31.13ºC) and CH_4 (-82.45ºC). At 25ºC, CO_2 adsorption takes place in subcritical conditions, i.e., it is susceptible to experience condensation processes in wide pores, whereas CH_4 adsorption takes place in supercritical conditions, i.e., it is non-condensable.

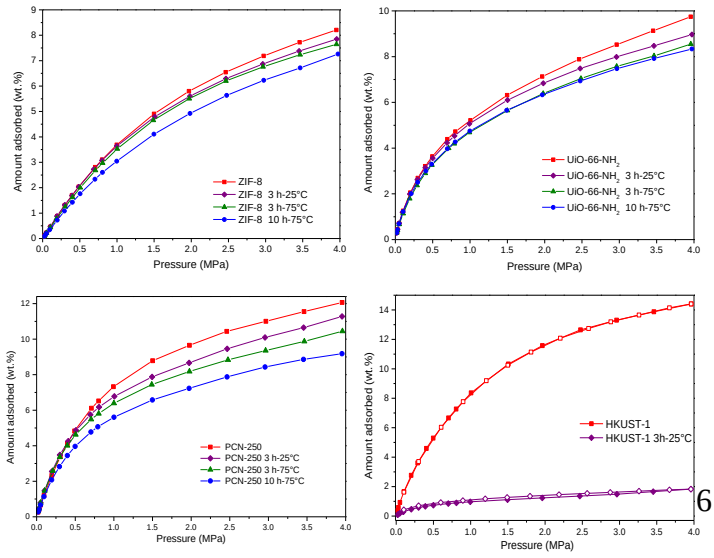

Figure 6. High-pressure CH_4 adsorption isotherms (wt.%) at 25ºC for ZIF-8, UiO-66-NH_2, PCN-250 and HKUST-1 before and after exposure to H_2S.

Figure 6 shows the high-pressure CH_4 isotherms for the four MOFs before and after the acid treatment. As expected, the largest adsorption capacity corresponded to the as-synthesized samples with a total capacity at 4.0 MPa around 8.2 wt.% for ZIF-8, 9.8 wt.% for UiO-66-NH_2, 12.1 wt.% for PCN-250 and 14.4 wt.% for HKUST-1 (see Tables S5-S8 for further details). These values are slightly lower than those described in the literature for the best carbon materials and MOFs (e.g., HKUST-1 with a capacity of 17-20 wt.% at 4.0 MPa).[11]

In all cases, exposure to H_2S gave rise to a decrease in the amount of CH_4 stored over the whole pressure range evaluated, this effect being rather similar at 2.0 MPa and 4.0 MPa. This observation reflects that CH_4 storage under these experimental conditions is affected by the amount and extend of micropores and not by the presence of wider pores. The decrease in the adsorption capacity was rather similar for ZIF-8 and UiO-66-NH_2 (around 15 % after the acid treatment at 75ºC for 10 h), whereas the effect for PCN-250 was much larger (around 25 %). In the specific case of HKUST-1, the decrease was close to 87%, with a final uptake close to 1.8 wt.%. These results are in agreement with the decrease in the micropore volume obtained from the N_2 isotherms after the H_2S treatment (Tables S1-S4). This decrease was around 11 % for ZIF-8 and UiO-66-NH_2, around 39 % for PCN-250 and 96% for HKUST-1. In any case, these results confirm that the effect of H_2S exposure in the CH_4 storage capacity is rather similar to the effect in CO_2 adsorption, at least at intermediate pressures. At high pressures, CO_2 can compensate and mitigate these detrimental effects due to the presence of mesoporosity available for CO_2 condensation at high pressures, whereas CH_4 does not.

Conclusion

The structural stability of four archetypical, well-faceted MOFs was evaluated upon exposure to an acidic environment. Experimental results showed that the structural deterioration depends on the nature of the MOF network (e.g., nature of the metallic nodes, hydrophilic properties, among others), and the crystallographic orientation of the exposed facets. While ZIF-8 exhibits a significant external deterioration on the crystal surface with the development of holes or cavities, FE-SEM images of UiO-66-NH_2 and PCN-250 does not allow to ascertain any on-surface structural damage. On the contrary, HKUST-1 exhibits a rather complete structural deterioration even after a treatment at 25ºC for 3h. XRPD and N_2 adsorption measurements confirmed the presence of a significant amorphization of the inner structure, mainly for ZIF-8 and PCN-250, associated with the preferential interaction of a soft base as sulphur with soft acid cations such as Fe(III) and Zn(II).

Notably, high-pressure adsorption measurements confirm that these structural changes have a dramatic effect in the adsorption performance of the four MOFs. Here, high-pressure CO_2 adsorption show that the structural deterioration and the associated decrease in the storage capacity is much larger for

HKUST-1, followed by ZIF-8 and PCN-250. The presence of -NH_2 functionalities and the lower affinity of Zr(IV) for sulphur limits the deterioration of the inner crystal structure of UiO-66-NH_2. However, the associated development of mesopores or holes in ZIF-8 and PCN-250 is able to compensate, at least partially, the detrimental effect of the acid treatment in the inner micropores. These observations suggest that, contrary to literature, the structural deterioration in ZIF-8 is not exclusively a surface phenomenon and some internal amorphization must take place, in close agreement with our XRPD measurements.
Contrariwise, high-pressure CH_4 adsorption confirm that the presence of acidic moieties in industrial streams will have a significant effect in the CH_4 storage capacity, mainly due to the deterioration of the inner microporous network. Although these drawbacks will be more drastic for MOFs with a large affinity between the metallic nodes and sulphur (such as HKUST-1 and PCN-250), we hypothesized that, in general, many MOFs will experience limitations to outperform under real industrial streams, unless guard beds are appropriately considered.

Experimental Section

Synthesis of MOFs

ZIF-8

ZIF-8 was synthesized according to a previously reported synthetic prodecure.[17] A solution of 0.3 g of $Zn(OAc)_2{\cdot}2H_2O$ in 5 mL of deionized water was added into a solution of 1.12 g of 2-methylimidazolate (2-MIM) in 5 mL of water, and the resulting mixture was homogenized by stirring it for a few seconds. Then, the mixture was let at room temperature for 24 h. White crystals were collected and washed several times with methanol and finally, dried under vacuum.

UiO-66-NH_2

A solution of 0.36 g of $ZrCl_4$ in 50 mL of DMF was added to a solution of 0.26 g of 2-aminoterephthalic acid and 35 mL of acid acetic glacial in 110 mL DMF. The resulting mixture was then heated at 120 ºC in an oven for 24 h. After this period, a crystalline powder was recovered by centrifugation, and washed twice with DMF and twice with MeOH.

Synthesis of 3,30,5,50-azobenzene tetracarboxylic acid (H_4-Tazb)

TazbH_4 was prepared following a previous procedure.[30] 9.5 g of 5-nitroisophthalic acid, 25 g of NaOH and 125 mL of distilled water were first placed into a 1 L 3-neck round bottom flask and stirred at 60 ºC for 1h. This mixture formed a pink slurry that turned yellow after 1 h. Meanwhile, 50 g of glucose were dissolved into 75 mL of distilled water at 60 ºC. The glucose solution was added slowly to the slurry, turning dark brown. The final mixture was left to cool down for 10 min, and air was bubbled into it for 16 h under stirring at room temperature. After this period, the mixture was cooled in an ice-bath and the sodium salt of Tazb recovered by filtration. The solid was then dissolved in 200 mL of distilled water and then, this solution was acidified to pH = 1, using 37% HCl, yielding a bright orange precipitate. The product was recovered by filtration, washed with distilled water and dried at 120 ºC.

PCN-250

PCN-250 was synthetized by a slight modification of the synthesis process previously described.[31] 0.56 g of NaOH was dissolved in 1 mL of distilled water. 2.0 g of H_4-TazBz were suspended in 11.12 mL of propan-2-ol. Both solutions were mixed at room temperature for 5 min. Meanwhile, 3.1 g of $FeCl_3{\cdot}6H_2O$ were dissolved at room temperature in 9 mL of propan-2-ol. Finally, the metal solution was added to the ligand solution, and the resulting slurry was stirred at 85 °C for 24 h. A crystalline powder was recovered by centrifugation, washed with distilled water and ethanol and dried under vacuum.

HKUST-1

For the synthesis of HKUST-1, a solution A was prepared by dissolving 0.420 g of benzene-1,3,5-tricarboxylic acid in 12 mL ethanol and a solution B was prepared by dissolving 0.8742 g of $Cu(NO_3)_2{\cdot}5H_2O$ in 12 mL of ultrapure water. Once dissolved, both solution were mixed under stirring conditions for 30 min, and later on transferred into a 50 mL teflon-lined stainless steel autoclave. The autoclave containing the mixture was placed in the oven at 110ºC for 18h. Finally, the obtained crystals were washed with ethanol and dried at 80ºC overnight.

H_2S exposure experiments

The synthesized MOFs were exposed to a flow of 1000 ppm H_2S in N_2 (30 ml/min) using an U-shaped quartz reactor. The acidic treatment was performed at two industrially relevant temperature conditions (25 ºC and 75 ºC) and for a total duration of 3 h. Note that, only at 75 ºC, the acidic treatment was extended to 10 h. The main purpose of this step was to expose MOF crystals to H_2S in the temperature range relevant to industrial biogas and flue gas streams, i.e. 25 ºC-75 ºC.

Physico-chemical characterization of the MOFs

Textural properties of the evaluated MOFs were determined using N_2 adsorption at cryogenic temperatures. N_2 data were obtained in a home-made manometric equipment designed and constructed by the LMA group and now commercialized by G2Mtech (www.g2mtech.com). Before the adsorption measurement, samples were outgassed under ultra-high vacuum conditions (UHV) for 4 h at 200 ºC. N_2 adsorption data were used to estimate the apparent surface area (S_{BET}), micropore volume (V_o), mesopore volume (V_{meso}) and total pore volume (V_T).

Powder X-Ray Diffraction (PXRD) patterns were recorded on an X'Pert PRO MPD analytical diffractometer (Panalytical) at 45 kV, 40 mA using CuKα radiation (λ = 1.5419 Å). Field-Emission Scanning Electron Microscopy (FE-SEM) images were collected on a FEI Magellan 400L scanning electron microscope at an acceleration voltage of 1.0 kV, using aluminum as support.

X-ray photoelectron spectroscopy (XPS) spectra were recorded in a XPS K-ALPHA Thermo Scientific. All spectra were collected using an Al-K radiation (1486.6 eV), monochromatized by a twin crystal monochromator, yielding focused X-ray spot elliptical shaped with a major axis length of 400 µm at 3 mA x 12 kV. The alpha hemispherical analyser was operated at the constant energy mode with survey scan pass energies of 200 eV to measure the whole energy band and 50 eV in a narrow scan to selectively measure the desired elements. Charge compensation was achieved with the system flood gun that provides low energy electrons and low energy argon ions from a single source. The CH_x in carbon 1s score level was used as reference binding energy (284.6 eV). The powder samples were pressed and mounted on the sample holder and placed in the vacuum chamber. Before the spectrum recording, the samples were maintained in the analysis chamber until a residual pressure of ca. 5×10^{-7} Nm^{-2}. The peaks deconvolution was performed by a quantitative analysis calculating the integral of each peak, after subtracting the S-shaped background, and by fitting the experimental curve to a combination of Lorentzian (30%) and Gaussian (70%) model. Due to the chemical heterogeneity of the MOF crystals after the H_2S treatment, XPS analysis have been performed in different

positions, the chemical composition reported in Table 1 being an average of these analyses.

High-pressure CO_2 and CH_4 measurements

High-pressure adsorption measurements were performed in a home-made fully automated equipment designed and constructed by the LMA group. Before the adsorption measurements, samples were outgassed *in-situ* under UHV conditions at 200 ºC for 4 h. Excess adsorption isotherms were obtained at 25ºC and up to 4.0 MPa for CH_4 and CO_2.

Acknowledgements

JSA would like to acknowledge financial support from the MINECO (Project MAT2016-80285-p). I.I. and D.M. would like to acknowledge financial support from the Spanish MINECO (Project RTI2018-095622-B-100), and Catalan AGAUR (Project 2017 SGR 238), the ERC, under the EU-FP7 (ERC-Co 615954) and the CERCA Program/Generalitat de Catalunya. ICN2 is supported by the Severo Ochoa Program from the Spanish MINECO (Grant No. SEV-2017-0706).

Keywords: MOFs • Acid exposure • Structural stability • H_2S • High-pressure

[1] J. Silvestre-Albero, F. Rodríguez-Reinoso in *Nanoporous Materials for gas Storage*, (Eds. K. Kaneko, F. Rodríguez-Reinoso), Green Energy and Technology Series, **2019**, pp. 209-226.

[2] M. Sevilla, G.A. Ferrero, A.B. Fuertes in *Nanoporous Materials for gas Storage*, (Eds. K. Kaneko, F. Rodríguez-Reinoso), Green Energy and Technology Series, **2019**, pp. 287-330.

[3] Y. He, W. Zhou, G. Qian, B. Chen, *Chem. Soc. Rev.* **2014**, *43*, 5657-5678.

[4] Y. Peng, V. Krungleviciute, I. Eryazici, J.T. Hupp, O.K. Farha, T. Yildirim, *J. Am. Chem. Soc.* **2013**, *135*, 11887-11894.

[5] B. Lin, H.-M. Wen, W. Zhou, J.Q. Xu, B. Chen, *Chem* **2016**, *1*, 557-580.

[6] A. Dailly, M. Beckner, in *Nanoporous Materials for gas Storage*, (Eds. K. Kaneko, F. Rodríguez-Reinoso), Green Energy and Technology Series, **2019**, pp. 227-253.

[7] Y. Ma, H. Tanaka, R. Matsuda in *Nanoporous Materials for gas Storage*, (Eds. K. Kaneko, F. Rodríguez-Reinoso), Green Energy and Technology Series, **2019**, pp. 331-358.

[8] J.H. Cavka, C.A. Grande, G. Mondino, R. Blom, *Ind. Eng. Chem. Res.* **2014**, *53*, 15500-15507.

[9] D. Britt, H. Furukawa, B. Wang, T. Grant Glover, O.M. Yaghi, J. Halpern, *PNAS* **2009**, *106*, 20637-20640.

[10] H. Li, K. Wang, Y. Sun, C.T. Lollar, J. Li, H.-C. Zhou, *Mater. Today* **2018**, *21*, 108-121.

[11] M.E. Casco, M. Martínez-Escandell, E. Gadea-Ramos, K. Kaneko, J. Silvestre-Albero, F. Rodríguez-Reinoso, *Chem. Mater.* **2015**, *27*, 959-964.

[12] J. Silvestre-Albero, A. Wahby, A. Sepúlveda-Escribano, M. Martínez-Escandell, K. Kaneko, F. Rodríguez-Reinoso, *Chem. Commun.* **2011**, *47*, 6840-6842.

[13] T. Tian, Z. Zeng, D. Vulpe, M.E. Casco, G. Divitini, P.A. Midgley, J. Silvestre-Albero, J.C. Tan, P.Z. Moghadam, D. Fairen-Jimenez, *Nature Materials* **2018**, *17*, 174-179.

[14] B.M. Connolly, M. Aragones-Anglada, J. Gandara-Loe, N.A. Danaf, D.C. Lamb, J.P. Mehta, D. Vulpe, S. Wuttke, J. Silvestre-Albero, P.Z. Moghadam, A.E.H. Wheatley, D. Fairen-Jimenez, *Nature Commun.* **2019**, *10*, 2345.

[15] S.H. Pang, C. Han, D.S. Sholl, C.W. Jones, R.P. Lively, *Chem. Mater.* **2016**, *28*, 6960-6967.

[16] A. Dutta, N. Tyminska, G. Zhu, J. Collins, R.P. Lively, J.R. Schmidt, S. Vasenkov, *J. Phys. Chem. C* **2018**, *122*, 7278-7287.

[17] C. Avci, J. Ariñez-Soriano, A. Carné-Sánchez, V. Guillerm, C. Carbonell, I. Imaz, D. Maspoch, *Angew. Chem. Int. Ed.* **2015**, *54*, 14417-14421.

[18] F. Rouquerol, J. Rouquerol, K.S.W. Sing in *Adsorption by Powders and Porous Solids*, Academic Press, **1999**.

[19] D. Fairen-Jimenez, S.A. Moggach, M.T. Wharmby, P.A. Wright, S. Parsons, T. Düren, *J. Am. Chem. Soc.* **2011**, *133*, 8900-8902.

[20] M.E. Casco, Y.Q. Cheng, L. Daemen, D. Fairen-Jimenez, E.V. Ramos-Fernandez, A.J. Ramirez-Cuesta, J. Silvestre-Albero, *Chem. Commun.* **2016**, *52*, 3639-3642.

[21] W.P. Mounfield, C. Han, S.H. Pang, U. Tumuluri, Y. Jiao, S. Bhattacharyya, M.R. Dutzer, S. Nair, Z. Wu, R.P. Lively, D.S. Sholl, K.S. Walton, *J. Phys. Chem. C* **2016**, *120*, 27230-27240.

[22] S. Bhattacharyya, S.H. Pang, M.R. Dutzer, R.P. Lively, K.S. Walton, D.S. Sholl, S. Nair, *J. Phys. Chem. C* **2016**, *120*, 27221-27229.

[23] Y.-C. Liang, C.-C. Wang, *RSC Advances* **2018**, *8*, 5063-5070.

[24] M.V. Morales-Gallardo, A.M. Ayala, M. Pal, M.A. Cortes Jacome, J.A. Toledo Antonio, N.R. Mathews, *Chem. Phys. Lett.* **2016**, *660*, 93-98.

[25] K. Xi, D. He, C. Harris, Y. Wang, C. Lai, H. Li, P.R. Coxon, S. Ding, C. Wang, R. Vasant Kumar, *Adv. Sci.* **2019**, *6*, 1800815.

[26] V. Presser, J. McDonough, S.-H. Yeon, Y. Gogotsi, *Energy Environ. Sci.* **2011**, *4*, 3059-3066.

[27] M.E. Casco, M. Martínez-Escandell, J. Silvestre-Albero, F. Rodríguez-Reinoso, *Carbon* **2014**, *67*, 230-235.

[28] H. Furukawa, N. Ko, Y.B. Go, N. Aratani, S.B. Choi, E. Choi, A.O. Yazaydin, R.Q. Snurr, M. O´Keeffe, J. Kim, O.M. Yaghi, *Science* **2010**, *329*, 424-428.

[29] A.R. Millward, O.M. Yaghi, *J. Am. Chem. Soc.* **2005**, *127*, 17998-17999.

[30] A. Dhakshinamoorthy, M. Alvaro, H. Chevreau, P. Horcajada, T. Devic, C. Serre, H. García, *Catal. Sci. Technol.* **2012**, *2*, 324-330.

[31] H. Chevreau, A. Permyakova, F. Nouar, P. Fabry, C. Livage, F. Ragon, A. García-Marquez, T. Devic, N. Steunou, C. Serre, P. Horcajada, *CrystEngComm.* **2016**, *18*, 4094-4104.

Entry for the Table of Contents

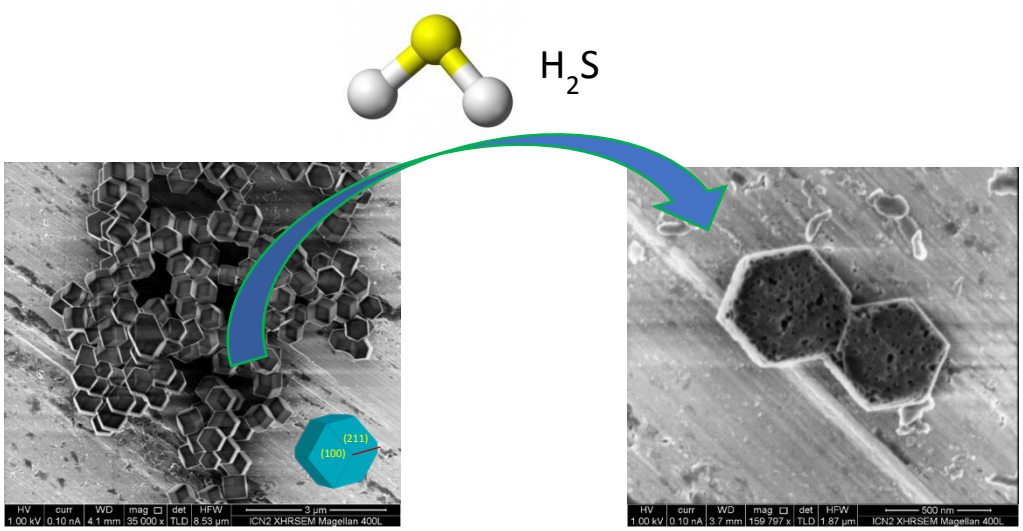

Well-faceted metal-organic frameworks

Internal/external deterioration upon H_2S exposure

Exposure of MOFs to an acidic environment (H_2S) give rise to important structural changes. Depending on the nature of the MOF and the crystallographic facets exposed, these changes include the development of cavities or holes in the external surface and/or the internal deterioration of the 3D MOF network. Furthermore, this structural deterioration gives rise to drastic changes in the adsorption performance of these materials for two relevant industrial processes: CO_2 capture and CH_4 storage.